SVM-Based Parameter Identification for Composite ZIP and Electronic Load Modeling

Chong Wang, *Member, IEEE*, Zhaoyu Wang, *Member, IEEE*, Jianhui Wang, *Senior Member, IEEE*, and Dongbo Zhao, *Senior Member, IEEE*

***Abstract*—This paper proposes a parameter identification technique for composite ZIP and electronic loads by leveraging the support vector machine (SVM) approach. Since the active power and the reactive power of electronic loads are piecewise functions of the voltage magnitude, the operating modes of electronic loads are determined by the voltage magnitude. To improve the accuracy of parameter identification, two filters (Hampel and Savitzky–Golay) are employed to preprocess measurements to reduce noise. The data after noise reduction serve as training data for the regression model that is solved by the SVM approach. Numerical results show that the SVM approach with filters can identify the parameters of the composite ZIP and electronic load model with high accuracy.**

Q1

***Index Terms*—Electronic load, noise reduction, parameter identification, support vector machine, ZIP load.**

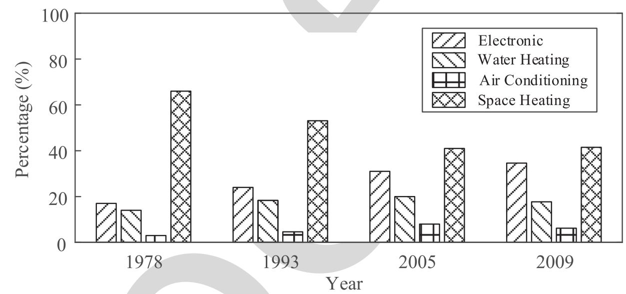

Fig. 1. Statistical data of typical energy consumption in homes by end uses in 1978, 1993, 2005, and 2009.

I. Introduction

LOAD modeling is important to power system analysis and control. Because more novel smart grid technologies such as power electronics are used in power systems, load modeling faces challenges from a variety of load components and a lack of detailed load information. Fig. 1 shows typical energy consumption in homes by end users in 1987, 1993, 2005, and 2009 [1], [2]. Statistical data show that electronic loads increased from 17% to 35% over that period, and new electronic devices continue to proliferate [3]. Since electronic devices continue to grow and the operating characteristics of these electronic devices are different from conventional loads such as space heating and water heating, their impacts must be included in models of when modeling load behavior.

The existing load modeling techniques can be classified into two broad categories: component-based models [4], [5] and measurement-based models. Component-based models explicitly represent physical characteristics of loads. However, it is a challenge to aggregate component-based models at the transmission -system level due to a lack of information about the load composition. Because more measurements can be obtained from phasor measurement units (PMUs) [6], [7], measurement-based models [8]–[14] have been used widely for load modeling. A measurement-based model has a generic representation without the need for detailed load characteristics. It is based on measurements from a specific location during a certain period, so it may not be suitable for other regions and other periods. It is also based on pre-specified load structures. For example, the ZIP model [15] and the exponential model [16] are usually used to relate active/reactive power to bus voltage, and the frequency dependent model [17] represents active/reactive power as bus voltage/frequency. These models only represent the static characteristics of loads. To include dynamic characteristics of loads, dynamic models such as the induction motor (IM) model [15] and the exponential recovery load model [18], [19] are usually used. These relate active/reactive power to bus voltage and time. In addition, composite models (e.g., the combination of the static models and the dynamic models) are employed to capture load behaviors accurately [20]–[23].

The operating characteristics of power electronics are different from conventional loads. Bonneville Power Administration (BPA) and the Western Electricity Coordinating Council (WECC) tested electronics such as variable-frequency drives and personal computers in their laboratories [24], [25]. The variable-frequency drives behave as constant power loads and trip at 60%–70% of voltage. The personal computers work as constant power loads that turn off at about 50% voltage and restart at about 60% voltage. Other electronics have similar operating characteristics. Based on these characteristics, WECC [25] and the North American Electric Reliability Corporation

Manuscript received June 11, 2017; revised March 5, 2018, May 9, 2018, and July 17, 2018; accepted August 12, 2018. This work was partially supported by the U.S. Department of Energy Office of Electricity Delivery and Energy Reliability, the Iowa Energy Center, Iowa Economic Development Authority and its utility partners. Paper no. TPWRS-01677-2017. *(Corresponding author: Zhaoyu Wang.)*

Q2

C. Wang and Z. Wang are with the Department of Electrical and Computer Engineering, Iowa State University, Ames, IA 50011 USA (e-mail: chongwang@hhu.edu.cn; wzy@iastate.edu).

J. Wang is with the Department of Electrical Engineering, Southern Methodist University, Dallas, TX 75205 USA (e-mail: jianhui@smu.edu).

D. Zhao is with Argonne National Laboratory, Lemont, IL 60439 USA (e-mail: dongbo.zhao@anl.gov).

Color versions of one or more of the figures in this paper are available online at http://ieeexplore.ieee.org.

Digital Object Identifier 10.1109/TPWRS.2018.2865966

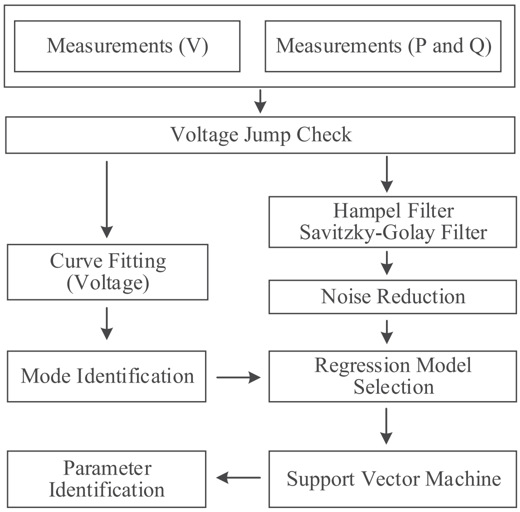

Fig. 2. Framework of the proposed method.

(NERC) [26] represent the models of electronics as piecewise functions with respect to bus voltage. These piecewise characteristics were not included in the existing studies [15]–[23].

Parameters of an appropriate load model are usually optimized by means of nonlinear least-squares (NLS) to achieve the minimum difference between the model outputs and the recorded measurements. Algorithms based on statistical techniques [27]–[29] and heuristic techniques [30]–[32] can be used to identify the parameters, and measurements with noise are usually directly used as algorithm inputs. However, potential outliers in measurements [33] may deviate parameter identification. In addition, current algorithms cannot deal with parameter identification for electronic models that are represented as piecewise functions.

To deal with the above-mentioned challenges, this paper proposes a SVM-based parameter identification approach for the composite ZIP and electronic load model. The main contributions of this paper are three-fold: (1) The operation characteristics of electronic loads are represented as piecewise functions with respect to voltage, and a composite ZIP and electronic load model is proposed. (2) Noise reduction techniques based on the Hampel filter and the Savitzky-Golay filter are used to reduce noise to improve the accuracy of parameter identification. (3) The SVM algorithm with the noise filters is used to identify the parameters of the composite load model.

The rest of the paper is organized as follows. Section II describes the framework of the proposed parameter identification for the ZIP and electronic load model. Section III presents composite ZIP and Electronic load modeling, and Section IV shows the algorithm for parameter identification. Section V shows the simulation results, and Section VI concludes the paper.

II. Framework of the Proposed Parameter Identification

Fig. 2 shows the framework of the proposed method. There are three key steps in this framework: mode identification, noise reduction, and parameter identification.

- *Mode identification:* Because power consumption of electronic loads can be expressed as a piecewise function of voltage magnitude, different voltage magnitudes may result in different operating modes. In this step, a voltage jump check is performed first, and then curve fitting is performed based on voltage measurements to obtain the operating modes according to the voltage magnitude. With the operating modes, the regression model of the composite ZIP and electronic load can be determined. The details are explained in the following sections.
- *Noise reduction:* Based on practical voltage measurements and power measurements, a new group of data after noise reduction will be employed as training data to improve the accuracy of parameter identification. The cleaned data are obtained by reducing noises from the practical measurements by means of the Hampel filter and the Savitzky-Golay filter.
- *Parameter identification:* Based on the new group of data after noise reduction, the support vector machine approach will be used to identify the parameters of the regression model of the composite ZIP and electronic load.

III. Composite ZIP and Electronic Load Modeling

This section first shows the mathematical formulation of the ZIP and electronic load model, and then shows the derivation of the regression model for the composite ZIP and electronic load model.

A. ZIP Model

The ZIP model is one of the typical static load models. It includes constant impedance (Z), constant current (I), and constant power (P). It is usually employed to represent the relationships between power and the voltage of interest. The mathematical formula is expressed as follows:

$$P_{ZIP,t} = P_{ZIP,0}\left(a_p\left(\frac{V_t}{V_0}\right)^2 + b_p\left(\frac{V_t}{V_0}\right) + c_p\right) \quad (1)$$

$$Q_{ZIP,t} = Q_{ZIP,0}\left(a_q\left(\frac{V_t}{V_0}\right)^2 + b_q\left(\frac{V_t}{V_0}\right) + c_q\right) \quad (2)$$

where $P_{ZIP,t}$ and $Q_{ZIP,t}$ are active power and reactive power, respectively, at the bus of interest at time t, V_0 is the nominal voltage, $P_{ZIP,0}$ and $Q_{ZIP,0}$ are base active/reactive power. V_t is the voltage magnitude at time t. a_p, b_p, and c_p are the parameters for active power of the ZIP load, and they satisfy $a_p + b_p + c_p = 1$. a_q, b_q, and c_q are the parameters for reactive power of the ZIP load, and they satisfy $a_q + b_q + c_q = 1$. The first term on the left side of (1) represents active power of the constant impedance load, and $P_{ZIP,0} \cdot a_p/V_0^2$ is the constant conductance. The second term on the left side of (1) represents the active power of the constant current load, and $P_{ZIP,0} \cdot b_p/V_0$ is the constant current. The third term represents active power of the constant power load, and $P_{ZIP,0} \cdot c_p$ is the constant power.

TABLE I
COEFFICIENT OF ELECTRONIC LOAD

Value of c_t	Condition	Mode
0	$V_t < V_{d2}$	1
$\frac{V_t - V_{d2}}{V_{d1} - V_{d2}}$	$V_{d2} \leq V_t < V_{d1}, V_t \leq V_{\min,t}$	2
$\frac{V_{\min,t} - V_{d2} + \alpha \cdot (V_t - V_{\min,t})}{V_{d1} - V_{d2}}$	$V_{d2} \leq V_t < V_{d1}, V_t > V_{\min,t}$	3
1	$V_t \geq V_{d1}, V_{\min,t} \geq V_{d1}$	4
$\frac{V_{\min,t} - V_{d2} + \alpha \cdot (V_{d1} - V_{\min,t})}{V_{d1} - V_{d2}}$	$V_t \geq V_{d1}, V_{\min,t} < V_{d1}$	5

B. Electronic Model

The electronic load defined in the software PowerWorld has the following characteristics:

- If the terminal voltage is higher than a threshold value V_{d1}, active power and reactive power of the electronic load are constant P and Q.
- If the voltage is between two threshold values V_{d1} and V_{d2} ($V_{d1} > V_{d2}$), the active power and reactive power of the electronic load are linearly reduced to zero.
- α represents a fraction of the electronic load. If α is larger than zero, it will be reconnected linearly as the voltage recovers.

The electronic load defined in the WECC composite load model is similar to that defined in PowerWorld, and its mathematical formula is expressed as follows:

$$P_{E,t} = c_t \cdot P_{E,0} \tag{3a}$$

$$Q_{E,t} = c_t \cdot Q_{E,0} \tag{3b}$$

where $P_{E,t}$ and $Q_{E,t}$ are active/reactive power of the electronic load at time t, $P_{E,0}$ and $Q_{E,0}$ are base active/reactive power, respectively. c_t is a coefficient related with the bus voltage, and it is listed in Table I. The modes depend on the terminal voltage.

In Table I, V_{d1} and V_{d2} are two threshold values, and α is a fraction of the electronic load that recovers from low voltage trip. $V_{\min,t}$ is a value tracking the lowest voltage but not below V_{d2}, and it is a known value at each sample. Its value can be expressed as follows:

$$V_{\min,t} = \max\{V_{d2}, \min\{V_t, V_{\min,t-1}\}\} \tag{4}$$

As shown in Table I, the mode of an electronic load depends on its terminal voltage. To illustrate the modes of the electronic load under different conditions, we show an example in Fig. 3. We assume that we have a voltage curve that is impacted not only by the load but also by the external grid, as shown in Fig. 3(a). Because $V_{\min,t}$ is defined to track the lowest voltage, its trajectory from t_1 to t_3 is the same as the trajectory of V_t in Fig. 3(a) because V_t decreases gradually over this period, as shown in Fig. 3(b). From t_3 to t_4, $V_{\min,t}$ keeps the value V_{d2} because it should not be less than V_{d2}. From t_4 to t_6, $V_{\min,t}$ maintains the value V_{d2} since V_{d2} is smaller than V_t.

Based on the conditions in Table I, as defined by WECC, the operating modes are determined according to voltage. Take the scenario in Fig. 3 as an example. From t_1 to t_2, because $V_t \geq V_{d1}$ and $V_{\min,t} \geq V_{d1}$, the electronic load is in Mode 4. From t_2 to t_3, the electronic model is in Mode 2 because $V_{d2} \leq V_t < V_{d1}$ and $V_t \leq V_{\min,t}$. From t_3 to t_4, the electronic load is in Mode 1 because the bus voltage is less that V_{d2}. From t_4 to t_5 and t_5 to t_6, the electronic load is in Mode 3 and Mode 5, respectively. In this research, we adopt the electronic load model defined by WECC.

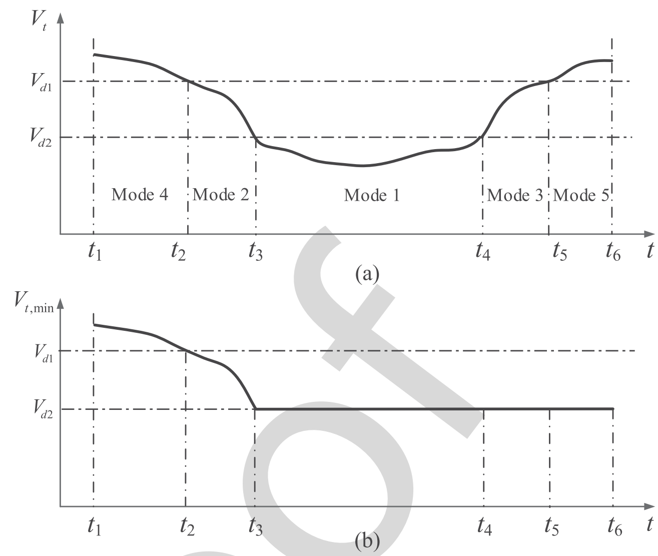

Fig. 3. (a) An example of bus voltage of an electronic load. (b) Trajectory of $V_{\min,t}$ at each sample. (The five modes are used for the sake of exposition, and the practical operation may not cover all five modes.)

For the component-level load, the voltage thresholds are known parameters. For an aggregate load that includes many electronic loads, we can first classify the electronic loads into different categories; the loads in a certain category share the same voltage thresholds. Then, we use the criteria in Table I to determine the mode of loads in each category, and obtain the formulations of the composite model's parameters in different modes. Because different categories have different thresholds, the mode of the aggregate load is the Cartesian product of the mode of each category.

C. Composite Model

With the ZIP model and the electronic load model, the composite model can be expressed as

$$P_t = (1 - \beta_p) \cdot P_{ZIP,t} + \beta_p \cdot P_{E,t} \tag{5a}$$

$$Q_t = (1 - \beta_q) \cdot Q_{ZIP,t} + \beta_q \cdot Q_{E,t} \tag{5b}$$

where β_p and β_q are the coefficients representing the portions of electronic loads in entire active/reactive power, respectively. P_t and Q_t are active/reactive power of the composite load, respectively.

According to (1) and (2), we know that active power and reactive power of the ZIP load are functions of V_t and V_t^2. In addition, active power and reactive power of the electronic load are functions of V_t according to (3a), (3b) and (4). We rewrite

TABLE II
PARAMETERS FOR ACTIVE POWER OF COMPOSITE MODEL

Mode	λ_1	λ_2	λ_3
1	$(1-\beta_p)\cdot\frac{P_{ZIP,0}\cdot a_p}{V_0^2}$	$(1-\beta_p)\cdot\frac{P_{ZIP,0}\cdot b_p}{V_0}$	$(1-\beta_p)\cdot P_{ZIP,0}\cdot c_p$
2	$(1-\beta_p)\cdot\frac{P_{ZIP,0}\cdot a_p}{V_0^2}$	$(1-\beta_p)\cdot\frac{P_{ZIP,0}\cdot b_p}{V_0}+\beta_p\cdot\frac{P_{E,0}}{V_{d1}-V_{d2}}$	$(1-\beta_p)\cdot P_{ZIP,0}\cdot c_p-\beta_p\cdot\frac{P_{E,0}\cdot V_{d2}}{V_{d1}-V_{d2}}$
3	$(1-\beta_p)\cdot\frac{P_{ZIP,0}\cdot a_p}{V_0^2}$	$(1-\beta_p)\cdot\frac{P_{ZIP,0}\cdot b_p}{V_0}+\beta_p\cdot\frac{P_{E,0}\cdot\alpha}{V_{d1}-V_{d2}}$	$(1-\beta_p)\cdot P_{ZIP,0}\cdot c_p+\beta_p\cdot\frac{P_{E,0}(V_{\min,t}-V_{d2}-\alpha\cdot V_{\min,t})}{V_{d1}-V_{d2}}$
4	$(1-\beta_p)\cdot\frac{P_{ZIP,0}\cdot a_p}{V_0^2}$	$(1-\beta_p)\cdot\frac{P_{ZIP,0}\cdot b_p}{V_0}$	$(1-\beta_p)\cdot P_{ZIP,0}\cdot c_p+\beta_p\cdot P_{E,0}$
5	$(1-\beta_p)\cdot\frac{P_{ZIP,0}\cdot a_p}{V_0^2}$	$(1-\beta_p)\cdot\frac{P_{ZIP,0}\cdot b_p}{V_0}$	$(1-\beta_p)\cdot P_{ZIP,0}\cdot c_p+\beta_p\cdot\frac{P_{E,0}(V_{\min,t}-V_{d2}+\alpha\cdot V_{d1}-\alpha\cdot V_{\min,t})}{V_{d1}-V_{d2}}$

(5a) and (5b) as

$$P_t = \lambda_1 \cdot V_t^2 + \lambda_2 \cdot V_t + \lambda_3 \tag{6a}$$

$$Q_t = \gamma_1 \cdot V_t^2 + \gamma_2 \cdot V_t + \gamma_3 \tag{6b}$$

where λ_1, λ_2, and λ_3 are the coefficients of active power, and the detailed formulations for these parameters in five modes are listed in Table II. The conditions for the five modes are the same as the conditions listed in Table I. γ_1, γ_2, and γ_3 are the coefficients of reactive power, and they have similar expressions to the coefficients of active power.

IV. ALGORITHMS FOR PARAMETER IDENTIFICATION

This section introduces voltage jump check, curve fitting for mode identification, noise filters for noise reduction, and a support vector machine for parameter identification.

A. Voltage Jump Check

Because we consider the steady-state model, we ignore the high-order dynamics of components. However, voltage may change a great deal due to different system conditions. This large change is considered a voltage jump. If we smooth the noise of all samples before and after the jump, the data after noise smoothing may be very different from the original sample. To deal with this, we analyze the voltage data and the power data together to check whether a voltage jump occurs. When a voltage jump occurs, the corresponding samples will not be used together to smooth noise. A voltage jump occurs when $|V_t - V_{t-1}|/V_{t-1} \geq V_G$ and $|P_t - P_{t-1}|/P_{t-1} \geq P_G$. V_t and V_{t-1} are voltage measurements at t and $t-1$, respectively. P_t and P_{t-1} are the real power measurements at t and $t-1$, respectively. V_G and P_G are the given threshold values. Because noises usually satisfy a normal distribution, about 99.7% of noises are within three standard deviations based on the 3-sigma rule. Because the values of voltage jumps are much larger than noise, V_G and P_G can be set to be larger than three standard deviations (e.g., six standard deviations).

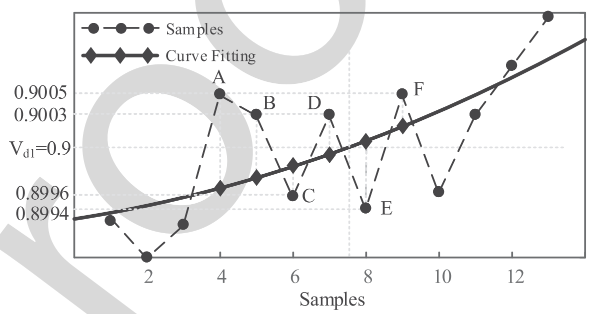

Fig. 4. A simple case for curve fitting.

B. Curve Fitting

Due to measurement noise, it is difficult to determine the operating modes when the measurements are close to the threshold values V_{d1} and V_{d2}. For example, samples A, B, C, D, E, and F in Fig. 4 are around the threshold V_{d1}. If we directly use the values of the samples A, B, C, D, E, and F to determine the modes, the operation shifts back and forth between two modes according to the mode criteria listed in Table I. The nosie may influence the mode selection. In practice, we should use the true values to identify modes. Hence, we first fit the curves of voltage around the threshold values V_{d1} and V_{d2} to help identify the modes. After curve fitting, samples A, B, C, and D are considered to belong to a mode, and samples E and F are considered to belong to another mode.

We use a polynomial function with an nth degree to fit the curve:

$$\hat{V}_t = c_0 + c_1 t + c_2 t^2 + \cdots + c_n t^n \tag{7}$$

where t is the sample time, and $c_0, \ldots, c_n$ are the coefficients. To find the coefficients, we can solve the problem:

$$\min \sum_t \left(V_t - \hat{V}_t\right)^2 \tag{8}$$

where V_t is the measurement at sample t. For this optimization, we can choose 50 samples around the threshold values V_{d1} and V_{d2} and a polynomial function with a third or fourth degree, and in this case overfitting will not occur. The model in (8) is

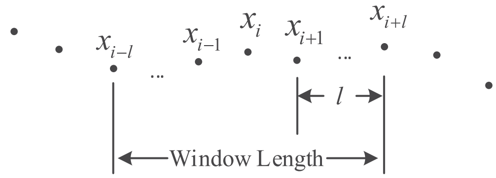

Fig. 5. Hampel filter.

a typical least-squares optimization model, which is solved by the curve fitting toolbox in Matlab.

C. Noise Filter

Noise in practical measurements has great impacts on parameter identification. Parameter identification for load modeling estimates the unknown parameters of the load model based on measurements. Noises and outliers impact the accuracy of the estimated parameters. To ensure high accuracy of parameter identification, a new group of data is derived based on the practical measurements by using filters. Because the Savitzky-Golay filter has an advantage in better preserving the amplitude of some high-frequency components and the Hampel filter has an advantage in robust outlier detection, these two filters are used to reduce noise.

1) Hampel Filter: The Hampel filter detects and removes noises and outliers by means of the Hampel identifier, and it depends on the three-sigma rule of statistics. For example, x_i in Fig. 5 has a median of a window including itself, and l adjacent samples on the two sides of x_i are calculated:

$$m_i = \mathrm{median}(x_{i-l}, \ldots, x_i, \ldots, x_{i+l}) \tag{9}$$

where m_i is the median, and l is the length of a sliding window, as shown in Fig. 5.

In addition, the standard deviation of each sample with respect to its window median is calculated by using the median absolute deviation:

$$MAD_i = \mathrm{median} \times (|x_{i-l} - m_i|, \ldots, |x_i - m_i|, \ldots, |x_{i+l} - m_i|) \tag{10}$$

$$\sigma_i = \kappa \cdot MAD_i \tag{11}$$

where σ_i is the standard deviation, and $\kappa = \frac{1}{\sqrt{2}\mathrm{erfc}^{-1} 1/2} \approx 1.4826$.

If the sample x_i satisfies the condition $|x_i - m_i| > N \cdot \sigma_i$, in which N is a given threshold, the sample x_i will be replaced by m_i.

2) Savitzky-Golay Filter: The Savitzky-Golay filter depends on the least-squares polynomial fitting through a moving window with the data in time domain, as shown in Fig. 6. For a sample x_i, we consider a polynomial with an nth degree:

$$y = c_0 + c_1(x - x_i) + c_2(x - x_i)^2 + \cdots + c_n(x - x_i)^n \tag{12}$$

where $c_0, c_1, \ldots, c_n$ are the coefficients. For the sample x_i associated with l samples to the left and l samples to the right, we

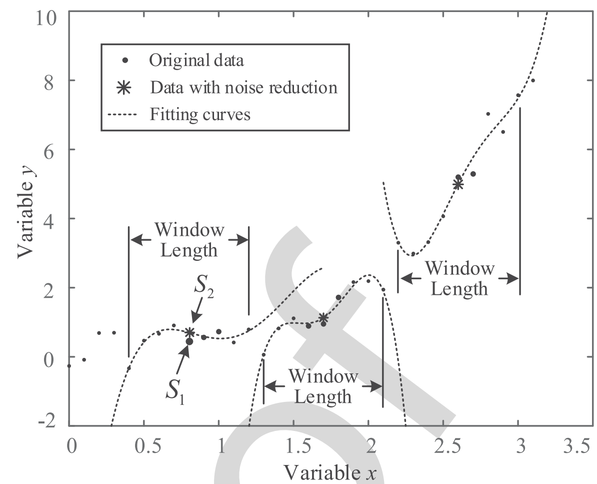

Fig. 6. Savitzky-Golay filter.

have $2l + 1$ equations:

$$\begin{aligned} y_{i-l} &= c_0 + c_1(x_{i-l} - x_i) + \cdots + c_n(x_{i-l} - x_i)^n \\ &\vdots \\ y_i &= c_0 \\ &\vdots \\ y_{i+l} &= c_0 + c_1(x_{i+l} - x_i) + \cdots + c_n(x_{i+l} - x_i)^n \end{aligned} \tag{13}$$

For these $2l + 1$ equations, the least-square approximated solution should be found. Equation (13) can be written in a matrix form as follows:

$$\begin{aligned} &\mathbf{A} \cdot \mathbf{c} = \mathbf{y} \\ &\mathbf{A} = \begin{bmatrix} 1 & x_{i-l} - x_i & \cdots & (x_{i-l} - x_i)^n \\ \vdots & \vdots & \vdots & \vdots \\ 1 & 0 & \cdots & 0 \\ \vdots & \vdots & \vdots & \vdots \\ 1 & x_{i+l} - x_i & \cdots & (x_{i+l} - x_i)^n \end{bmatrix} \\ &\mathbf{c} = \begin{bmatrix} c_0 & c_1 & \cdots & c_n \end{bmatrix}^T \\ &\mathbf{y} = \begin{bmatrix} y_{i-l} & \cdots & y_i & \cdots & y_{i+l} \end{bmatrix}^T \end{aligned} \tag{14}$$

where the superscript T denotes matrix/vector transpose. The least-squares solution for (14) is derived by using the following formula:

$$\mathbf{c} = (\mathbf{A}^T \cdot \mathbf{A})^{-1} \cdot (\mathbf{A}^T \cdot \mathbf{y}) \tag{15}$$

The value c_0 works as a new data after noise reduction. For example, the sample S_1 is the original sample, and S_2 is the data after noise reduction with the Savitzky-Golay filter. Because the Savitzky-Golay filter is a filter through a moving window with the measurements in a time domain, we will stop the fit after the last measurement in time domain is processed by the filter.

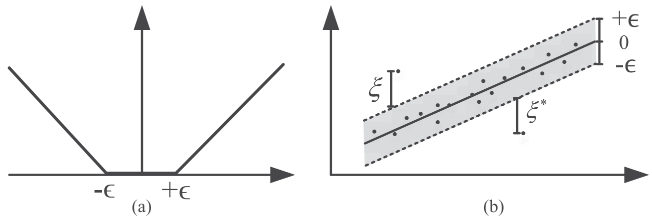

Fig. 7. (a) Vapnik ϵ-insensitive loss objective for SVM regression estimation. (b) Use of slack variables ξ and ξ^* for points that cannot satisfy the ϵ accuracy.

D. Support Vector Machine for Linear Regression

This section first presents the basic model of the support vector machine approach for the linear regression, and then shows its dual model and its quadratic program.

1) Basic Model of Support Vector Machine: It is assumed that we have data $\{(\mathbf{x}_1, y_1), \dots, (\mathbf{x}_N, y_N)\}$, and the regression of the data can be written as follows:

$$y_i = \mathbf{k}^T \mathbf{x}_i + b \tag{16}$$

where y_i, $b \in \mathbb{R}$, $\mathbf{k}$, $\mathbf{x}_i \in \mathbb{R}^n$, and $i \in \{1, \dots, N\}$. The estimated parameters $\mathbf{k}$ and b can be found by minimizing the empirical risk of training data. One typical objective for estimation is the squared error defined as follows:

$$\min \quad \sum_i \left(y_i - \mathbf{k}^T \mathbf{x}_i - b\right)^2 \tag{17}$$

For the standard SVM regression, a ϵ-insensitive loss objective proposed by Vapnik is used:

$$\begin{aligned} &\left|y_i - \mathbf{k}^T \mathbf{x}_i - b\right|_\epsilon \\ &= \begin{cases} 0, & \text{if} \left|y_i - \mathbf{k}^T \mathbf{x}_i - b\right| \le \epsilon \\ \left|y_i - \mathbf{k}^T \mathbf{x}_i - b\right| - \epsilon, & \text{otherwise} \end{cases} \end{aligned} \tag{18}$$

where ϵ denotes the accuracy required by users, as shown in Fig. 7. Theoretically, the SVM approach can be applied to any convex objective function. In general, a 1-norm objective is more robust than a 2-norm objective (e.g., when dealing with non-Gaussian nosie on training data).

For the ϵ-insensitive loss objective, we expect to find one function that is as flat as possible has the largest deviation ϵ. One way to guarantee this is to minimize the Euclidean norm (i.e., $\mathbf{k}^T \mathbf{k}$) with some linear constraints, as follows:

$$\min \quad \frac{1}{2}\mathbf{k}^T \mathbf{k} \tag{19a}$$

$$\text{s.t.} \quad y_i - \mathbf{k}^T \mathbf{x}_i - b \le \epsilon \qquad \forall i \tag{19b}$$

$$\mathbf{k}^T \mathbf{x}_i + b - y_i \le \epsilon \qquad \forall i \tag{19c}$$

However, some points may be beyond the constraints in (19). Similar to the soft margin employed in SVM by Vapnik and Cortes [34], slack variables ξ_i and ξ_i^* are introduced to deal with infeasible constraints in (19), and the optimization model can be rewritten as follows:

$$\min \quad \frac{1}{2}\mathbf{k}^T \mathbf{k} + C \sum_{i=1}^{N} (\xi_i + \xi_i^*) \tag{20a}$$

$$\text{s.t.} \quad y_i - \mathbf{k}^T \mathbf{x}_i - b \le \epsilon + \xi_i \quad \forall i \tag{20b}$$

$$\mathbf{k}^T \mathbf{x}_i + b - y_i \le \epsilon + \xi_i^* \quad \forall i \tag{20c}$$

$$\xi_i, \xi_i^* \ge 0 \qquad \forall i \tag{20d}$$

where the constant $C > 0$ is a parameter, which determines the trade off between the flatness of the regression function and the tolerance of deviations greater than ϵ, as illustrated in Fig. 7(b).

2) Dual Model and Quadratic Programming: The optimization model (20) is complex due to the high dimensionality of the input space. Therefore, its dual model is used to obtain the optimal solution. A Lagrangian function with respect to the constraints and the original objective is first established by introducing a group of dual variables, as follows:

$$\begin{aligned} L(\mathbf{k}, b, \xi_i, \xi_i^*, \beta_i, \beta_i^*, \eta_i, \eta_i^*) &= \frac{1}{2}\mathbf{k}^T \mathbf{k} + C \sum_{i=1}^{N} (\xi_i + \xi_i^*) \\ &- \sum_{i=1}^{N} \beta_i \left(\epsilon + \xi_k - y_i + \mathbf{k}^T \mathbf{x}_i + b\right) \\ &- \sum_{i=1}^{N} \beta_i^* \left(\epsilon + \xi_k^* + y_i - \mathbf{k}^T \mathbf{x}_i - b\right) \\ &- \sum_{i=1}^{N} (\eta_i \xi_i + \eta_i^* \xi_i^*) \end{aligned} \tag{21}$$

where L is the Lagrange function, and β_i, β_i^*, η_i, and η_i^* are Lagrangian multipliers that satisfy the following constraints.

$$\beta_i, \beta_i^*, \eta_i, \eta_i^* \ge 0 \quad \forall i \tag{22}$$

For the Lagrangian function in (21), the primal and dual variables at the solution correspond to a saddle point [35]. The saddle point can be characterized as follows:

$$\max_{\beta_i, \beta_i^*, \eta_i, \eta_i^*} \ \min_{\mathbf{k}, b, \xi_i, \xi_i^*} \ L(\mathbf{k}, b, \xi_i, \xi_i^*, \beta_i, \beta_i^*, \eta_i, \eta_i^*) \tag{23}$$

with conditions for optimal solution.

$$\frac{\partial L}{\partial \mathbf{k}} = \mathbf{k} - \sum_{i=1}^{N} (\beta_i - \beta_i^*)\mathbf{x}_i = 0 \tag{24a}$$

$$\frac{\partial L}{\partial b} = \sum_{i=1}^{N} (\beta_i - \beta_i^*) = 0 \tag{24b}$$

$$\frac{\partial L}{\partial \xi_i} = C - \beta_i - \eta_i = 0 \quad \forall i \tag{24c}$$

$$\frac{\partial L}{\partial \xi_i^*} = C - \beta_i^* - \eta_i^* = 0 \quad \forall i \tag{24d}$$

TABLE III
PARAMETERS OF COMPOSITE LOAD

Parameters	Values (p.u.)	Parameters	Values (p.u.)
$P_{ZIP,0}$	0.80	$Q_{ZIP,0}$	0.40
a_p	0.20	b_p	0.40
c_p	0.40	a_q	0.15
b_q	0.35	c_q	0.50
V_{d1}	0.95	V_{d2}	0.70
α	0.25	$P_{E,0}$	0.45
$Q_{E,0}$	0.30	β	0.40
V_0	1.00		

Substituting (24a), (24b), (24c), and (24d) to (21) produces the dual optimization model.

$$\max_{\beta_i,\beta_i^*} \quad -\frac{1}{2}\sum_{i=1}^{N}\sum_{j=1}^{N}(\beta_i-\beta_i^*)(\beta_j-\beta_j^*)\mathbf{x}_i^T\mathbf{x}_j - \epsilon\sum_{i=1}^{N}(\beta_i+\beta_i^*)+\sum_{i=1}^{N}y_i(\beta_i-\beta_i^*) \tag{25a}$$

$$\text{s.t.} \quad \sum_{i=1}^{N}(\beta_i-\beta_i^*)=0 \tag{25b}$$

$$0\leq\beta_i,\beta_i^*\leq C \quad \forall i \tag{25c}$$

The Lagrangian multipliers β_i and β_i^* can be obtained by solving the quadratic optimization model (25a), (25b), and (25c). Then, parameter $\mathbf{k}$ can be described as a linear combination of the training data with the condition (24a) as follows:

$$\mathbf{k}=\sum_{i=1}^{N}(\beta_i-\beta_i^*)\mathbf{x}_i \tag{26}$$

V. CASE STUDIES

This section validates the proposed parameter identification approach for the composite ZIP and electronic loads. The effectiveness of the proposed method is verified by the case studies, and the sensitivities of the approaches to outliers are compared.

A. Data Description

A revised IEEE 123-bus system [36] is employed for simulations. To illustrate the results, we focus on the measurements of bus 6, which is connected with a composite ZIP and electronic load. The detailed parameters for the composite load are shown in Table III. To test the model and the identification algorithm, 1,000 operating points are simulated to obtain the true values including voltage and power. Then, noises are added to the true values in p.u. to generate the signals. The noises are assumed to satisfy a Gaussian distribution with zero mean and a standard deviation of 0.001. To compare the results, we consider 1,000 scenarios, each of which has 1,000 signals with different noise added to the true values. The number of samples for curve fitting around the threshold values is 50. The threshold values of V_G and P_G for checking voltage jumps are both set to 0.05 (p.u.).

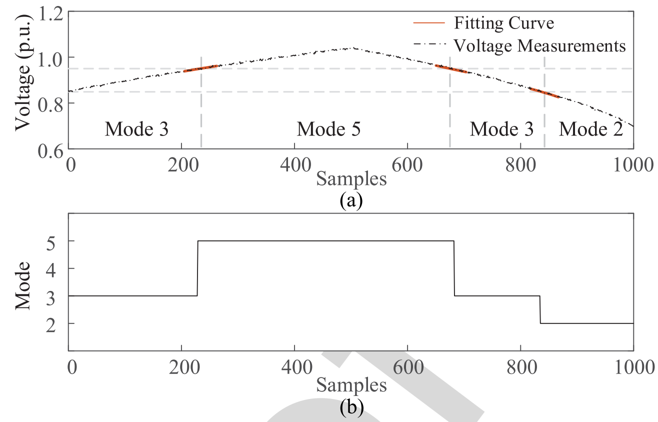

Fig. 8. (a) Voltage measurements and fitting curve. (b) Operating modes for different samples.

TABLE IV
ESTIMATIONS OF λ_1, λ_2, AND λ_3 UNDER DIFFERENT MODES FOR SIMULATED DATA

		True Value	SVM	H-SVM	SG-SVM
Mode 3	λ_1	0.0960	0.1025	0.0995	0.0989
	λ_2	0.3720	0.3602	0.3656	0.3666
	λ_3	0.1503	0.1556	0.1531	0.1527
Mode 5	λ_1	0.0960	0.1004	0.0985	0.0981
	λ_2	0.1920	0.1833	0.1871	0.1878
	λ_3	0.3213	0.3256	0.3237	0.3234
Mode 2	λ_1	0.0960	0.1028	0.0990	0.0986
	λ_2	0.9120	0.9012	0.9072	0.9078
	λ_3	-0.3120	-0.3077	-0.3101	-0.3103

The lengths of the noise filers are set to be 5. The order of the Savitzky-Golay filter is three. Because the order of the filter is three (i.e., a polynomial function with a thrid degree is used) and the length of the filter is five (i.e., five samples are used), it will not be overfitting.

To identify the load parameters, the modes should be determined first. Fig. 8(a) shows the signals of one scenario. The black dots represent the voltage measurements, and the red line is the fitting curve of the voltage around the threshold values of V_G and P_G. Fig. 8(b) shows the modes of the bus of interest in the analysis period. There are three modes: mode 2, mode 3, and mode 5.

B. Effectiveness of Proposed Method

Table IV shows the estimate of λ_1, λ_2, and λ_3 under different modes. It is observed that the results based on SVM with the Savitzky-Golay filter (SG-SVM) are the closest to the true values and the results based on SVM with the Hampel filter (H-SVM) are the second closest to the true values. Fig. 9 shows the probability density function (PDF) of relative errors (REs) of the parameter λ_1 by using different algorithms. The mean values of REs with SVM, H-SVM, and SG-SVM are 6.79%,

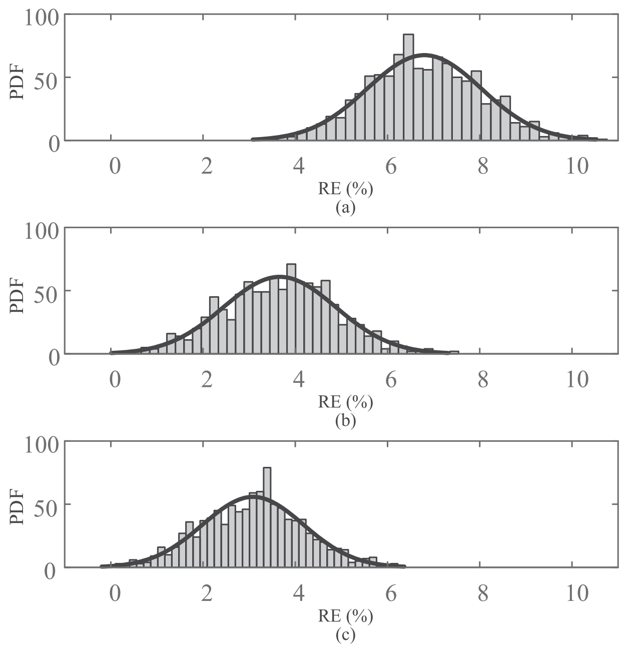

Fig. 9. Probability density functions of relative errors of λ_1 using (a) SVM, (b) H-SVM, and (c) SG-SVM.

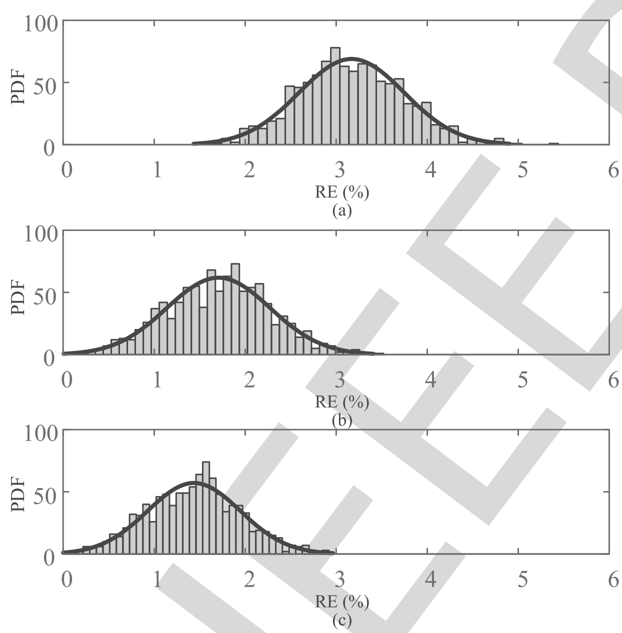

Fig. 10. Probability density functions of relative errors of λ_2 using (a) SVM, (b) H-SVM, and (c) SG-SVM.

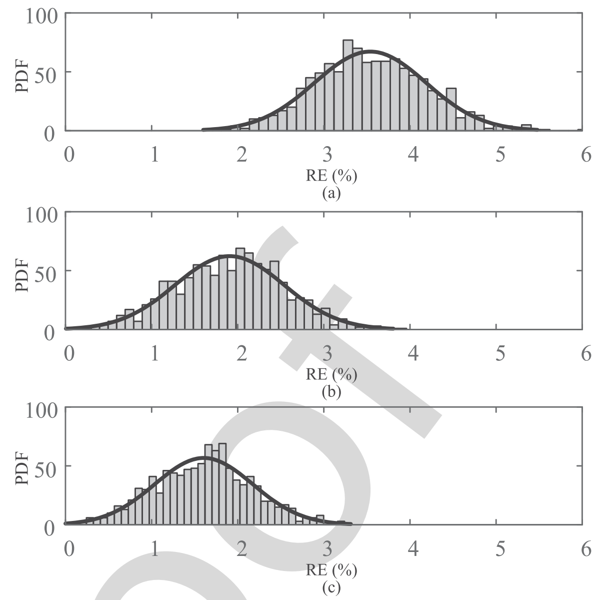

Fig. 11. Probability density functions of relative errors of λ_3 by using (a) SVM, (b) H-SVM, and (c) SG-SVM.

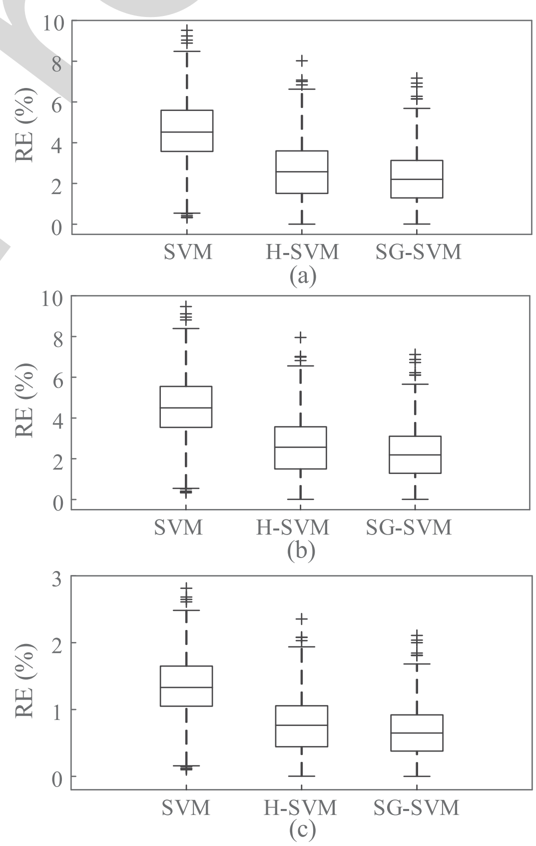

Fig. 12. REs of the parameters (a) λ_1, (b) λ_1, and (c) λ_1 under mode 5.

3.66%, and 3.08%, respectively. Fig. 10 shows the REs' PDF of the parameter λ_2 with different algorithms. The mean values of REs with SVM, H-SVM, and SG-SVM are 3.17%, 1.71%, and 1.42%, respectively. Fig. 11 shows the REs' PDF of the parameter λ_3 by means of different algorithms. The mean values of REs with SVM, H-SVM, and SG-SVM are 3.54%, 1.91%, and 1.60%, respectively.

Fig. 12 shows REs of the parameters λ_1, λ_2, and λ_3 under mode 5 using different algorithms. The mean values of REs of the estimated λ_1 with SVM, H-SVM, and SG-SVM are 4.56%, 2.64%, and 2.29%, respectively. For the estimated λ_2,

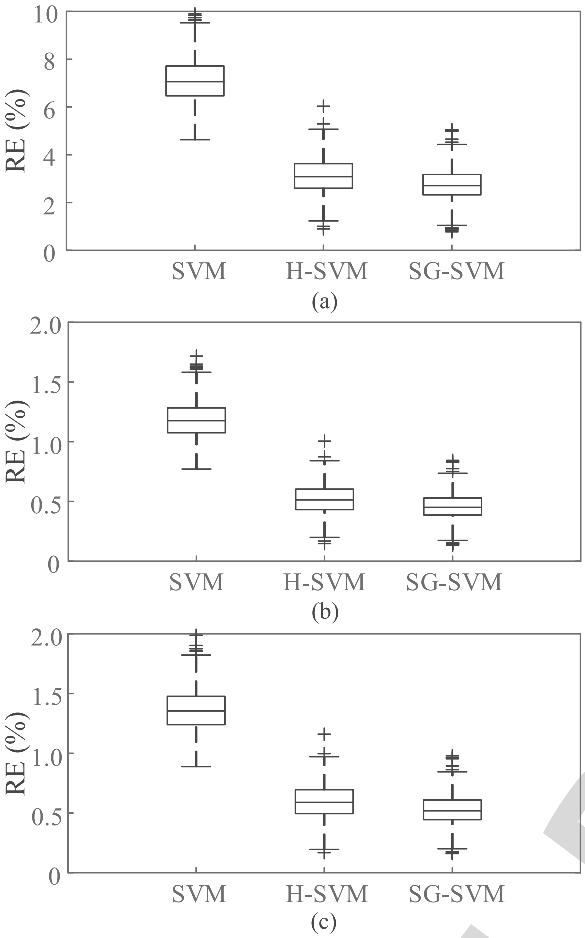

Fig. 13. REs of the parameters (a) λ_1, (b) λ_1, and (c) λ_1 under mode 2.

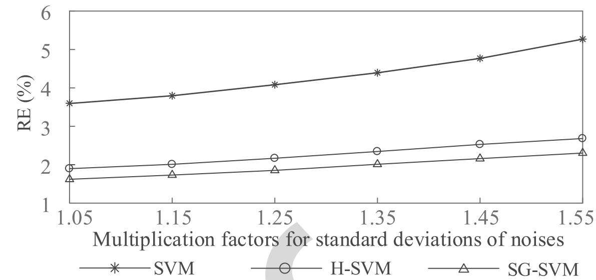

Fig. 14. REs with increased standard deviations of noises.

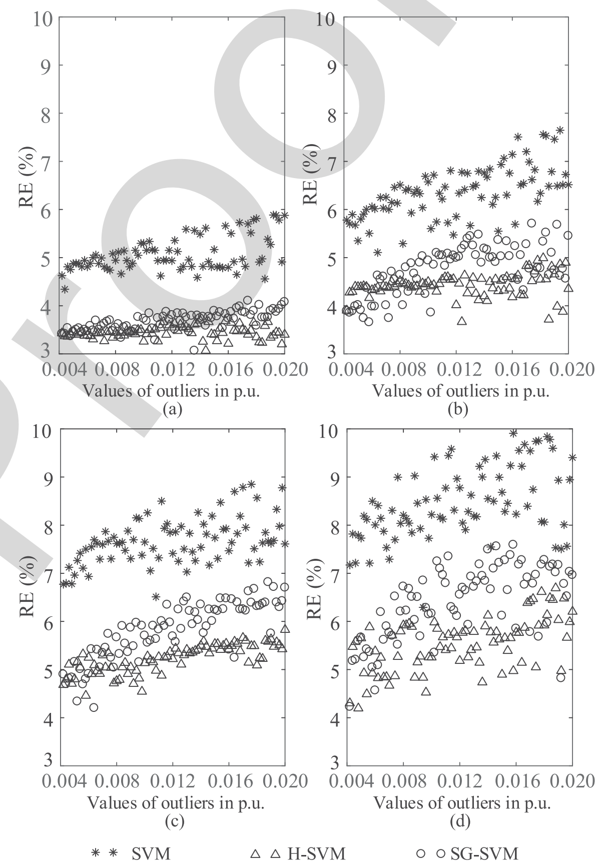

Fig. 15. (a) Relative errors when outliers' rate is 1%. (b) Relative errors when outliers' rate is 2%. (c) Relative errors when outliers' rate is 3%. (d) Relative errors when outliers' rate is 4%.

the mean values of REs with SVM, H-SVM, and SG-SVM are 4.53%, 2.62%, and 2.27%, respectively. For the estimated λ_3, the mean values of REs are 1.34%, 0.77%, and 0.67%, respectively. Fig. 13 shows the results under the mode 2 with different algorithms. The mean values of REs of the estimated λ_1 with SVM, H-SVM, and SG-SVM are 7.10%, 3.13%, and 2.75%, respectively. For the estimated λ_2, the mean values of REs with SVM, H-SVM, and SG-SVM are 1.18%, 0.52%, and 0.45%, respectively. For the estimated λ_3, the mean values of REs with SVM, H-SVM, and SG-SVM are 1.36%, 0.59%, and 0.52%, respectively. Based on these results, we can conclude that SG-SVM has the best performance, followed by H-SVM, and SVM has the worst performance.

Fig. 14 shows REs with different standard deviations of noise. Even though the standard deviations of noise increase, the results using H-SVM and SG-SVM have lower REs. In addition, outliers may be associated with measurements, and the capability to deal with these outliers is critical. Fig. 15 shows REs of λ_1 of mode 3 by using different approaches with different outlier rates. H-SVM has the best performance in dealing with outliers, followed by SG-SVM, and SVM has the worst performance.

To further test the algorithm, additional voltage curves are used. The test system and the parameters are the same as the scenario in Fig. 8. The new voltage curve and the corresponding modes are shown in Fig. 16. In this test, we consider a voltage jump scenario. To guarantee that the voltage jump is not an outlier associated with the voltage measurements, we also check power data. If they both have jumps, the corresponding data will not be considered an outlier. In this case, the measurements before and after the jump will not be used together to smooth noise. For this test, we have four modes. Table V shows REs of the estimated parameters with different approaches. This test shows that SG-SVM has the best performance to deal with outliers, followed by H-SVM, and SVM has the worst performance.

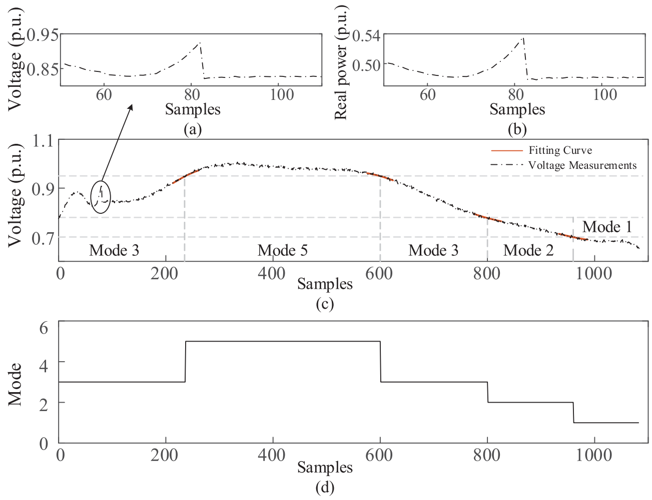

Fig. 16. (a) Part of voltage curve. (b) Part of power curve. (c) Voltage curve. (d) Operating modes at different samples.

TABLE V
REs of Estimated Parameters with Different Approaches Under Modes for Simulated Data

		RE(%)		
		λ_1	λ_2	λ_3
Mode 3	SVM	3.8096	3.7222	1.2502
	H-SVM	1.4945	1.4567	0.4881
	SG-SVM	1.3425	1.3081	0.4382
Mode 5	SVM	3.2434	1.4514	2.1558
	H-SVM	2.2573	1.0089	1.4973
	SG-SVM	1.9042	0.8514	1.2642
Mode 2	SVM	3.7946	2.4658	2.1368
	H-SVM	2.6245	1.6136	1.3539
	SG-SVM	1.8349	1.1489	0.9387
Mode 1	SVM	4.2486	4.3978	3.1454
	H-SVM	2.9223	2.1284	1.8354
	SG-SVM	1.5445	1.4543	1.1254

The above sample measurements are based on simulations. To further validate the model and the algorithm, we also used Chroma Programmable AC/DC Electronic Load 63804 and Manual Variable Transformer R42207 to generate experimental data. With different modes, the power is equivalent to a constant impedance load, a constant current load, and a constant power load. This can be programed using Chroma Programmable AC/DC Electronic Load, and Manual Variable Transformer R42207 is used to generate the terminal variable voltage. Fig. 17 shows voltage and power. In this test, $P_{ZIP,0} = 800$ W, $P_{E,0} = 400$ W, $V_0 = 200$ V, $V_{d1} = 209$, $V_{d2} = 154$, $a_p = 0.2$, $b_p = 0.4$, $c_p = 0.4$, $\alpha = 0.25$, and $\beta_p = 0.2$. There are four modes: mode 4, mode 2, mode 1, and mode 3. Table VI shows

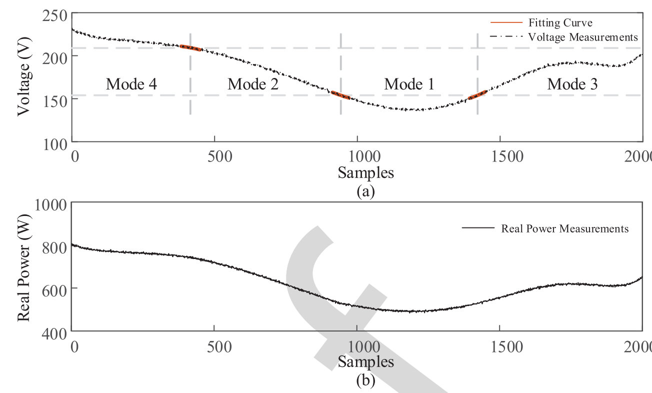

Fig. 17. (a) Voltage curve. (b) Power curve.

TABLE VI
REs of Estimated Parameters with Different Approaches Under Modes for Experimental Data

		RE(%)		
		λ_1	λ_2	λ_3
Mode 4	SVM	5.1011	5.5973	2.3383
	H-SVM	3.6899	4.0456	1.6889
	SG-SVM	3.3067	3.6281	1.5158
Mode 2	SVM	2.8268	1.2071	9.3492
	H-SVM	2.6826	1.1472	8.8973
	SG-SVM	2.3242	0.9923	7.6816
Mode 1	SVM	4.8501	3.5064	1.2659
	H-SVM	3.8437	2.7783	1.0029
	SG-SVM	3.4770	2.5142	0.9079
Mode 3	SVM	3.2761	2.2586	1.6355
	H-SVM	3.1485	2.1709	1.5727
	SG-SVM	2.8219	1.9386	1.3997

REs of the parameters. SG-SVM has the best performance to deal with noise, followed by H-SVM, and SVM has the worst performance.

VI. Conclusions

This paper focuses on parameter identification for the composite ZIP and electronic load by using the support vector machine (SVM) approach. Because the power consumption of the electronic load is a piecewise function of voltage magnitude, the approximated voltage curve, which determines the operating modes of the electronic loads, is achieved by using the curve fitting approach. To improve the accuracy of parameter identification, two filters (i.e., the Hampel filter and the Savitzky-Golay filter) are employed to preprocess measurements to reduce noises before using the SVM approach. Several tests were used to validate the model and the method. The major findings are as follows: (1) SG-SVM has the best performance to deal with noise, followed by H-SVM, and SVM has the worst performance. (2) H-SVM has the best performance to deal with outliers, followed by SG-SVM, and SVM has the worst performance.

Usually, one critical factor determining the data quality is the measurement unit. In practice, we can analyze the historical data from the measurement unit. If the measurements from the unit have a high rate of outliers, H-SVM can be selected. If the measurements from the unit have a very low rate of outliers, we can select SG-SVM.

References

[1] U.S. Energy Information Administration, "Share of Energy Used by Appliances and Consumer Electronics Increases in U.S. Homes," 2011. [Online]. Available: https://www.eia.gov/consumption/residential/reports/2009/electronics.php

[2] U.S. Energy Information Administration, "Heating and Cooling No Longer Majority of U.S. Home Energy Use," 2013. [Online]. Available: https://www.eia.gov/todayinenergy/detail.php?id=10271#

[3] Electric Power Research Institute, "Consumer Electronics and Motorized Appliances," 2015. [Online]. Available: http://www.energy.ca.gov/2016publications/CEC-500-2016-034/CEC-500-2016-034.pdf

[4] I. Dzafic, M. Glavic, and S. Tesnjak, "A component-based power system model-driven architecture," *IEEE Trans. Power Syst.*, vol. 19, no. 4, pp. 2109–2110, Nov. 2004.

[5] D. Kosterev *et al.*, "Load modeling in power system studies: WECC progress update," in *Proc. IEEE Power Energy Soc. Gen. Meeting*, Pittsburgh, PA, USA, Jul. 2008, pp. 1–8.

Q3 [6] *IEEE Standard for Synchrophasor Measurements for Power Systems*, IEEE Standard C37.118.1-2011 (Revision of IEEE Standard C37.118-2005), pp. 1–61, Dec. 2011.

[7] R. R. Mohassel, A. Fung, F. Mohammadi, and K. Raahemifar, "A survey on advanced metering infrastructure," *Int. J. Elect. Power Energy Syst.*, vol. 63, pp. 473–484, Dec. 2014.

[8] H. Renmu, M. Jin, and D. J. Hill, "Composite load modeling via measurement approach," *IEEE Trans. Power Syst.*, vol. 21, no. 2, pp. 663–672, May 2006.

[9] J. Ma, D. Han, R. M. He, Z. Y. Dong, and D. J. Hill, "Reducing identified parameters of measurement-based composite load model," *IEEE Trans. Power Syst.*, vol. 23, no. 1, pp. 76–83, Feb. 2008.

[10] I. F. Visconti, D. A. Lima, J. M. C. de Sousa Costa, and N. R. de B. C. Sobrinho, "Measurement-based load modeling using transfer functions for dynamic simulations," *IEEE Trans. Power Syst.*, vol. 29, no. 1, pp. 111–120, Jan. 2014.

[11] D. Han, J. Ma, R. He, and Z. Dong, "A real application of measurement-based load modeling in large-scale power grids and its validation," *IEEE Trans. Power Syst.*, vol. 24, no. 4, pp. 1756–1764, Nov. 2009.

[12] C. Wang, B. Cui, and Z. Wang, "Analysis of solvability boundary for droop-controlled microgrids," *IEEE Trans. Power Syst.*, to be published.

Q4 [13] C. Wang, Z. Wang, J. Wang, and D. Zhao, "Robust time-varying parameter identification for composite load modeling," *IEEE Trans. Smart Grid*, to be published.

[14] A. Arif, Z. Wang, J. Wang, B. Mather, H. Bashualdo, and D. Zhao, "Load modeling—A review," *IEEE Trans. Smart Grid*, to be published.

[15] P. Kundur, *Power System Stability and Control*, New York, NY, USA: McGraw-Hill, 1994.

[16] K.-H. Tseng, W.-S. Kao, and J.-R. Lin, "Load model effects on distance relay settings," *IEEE Trans. Power Del.*, vol. 18, no. 4, pp. 1140–1146, Oct. 2003.

[17] "Standard load models for power flow and dynamic performance simulation," *IEEE Trans. Power Syst.*, vol. 10, no. 3, pp. 1302–1313, Aug. 1995.

Q5 [18] D. J. Hill, "Nonlinear dynamic load models with recovery for voltage stability studies," *IEEE Trans. Power Syst.*, vol. 8, no. 1, pp. 166–176, Feb. 1993.

[19] W. Xu and Y. Mansour, "Voltage stability analysis using generic dynamic load models," *IEEE Trans. Power Syst.*, vol. 9, no. 1, pp. 479–493, Feb. 1994.

[20] Y. Ge, A. J. Flueck, D. K. Kim, J. B. Ahn, J. D. Lee, and D. Y. Kwon, "An event-oriented method for online load modeling based on synchrophasor data," *IEEE Trans. Smart Grid*, vol. 6, no. 4, pp. 2060–2068, Jul. 2015.

[21] W.-S. Kao, C.-J. Lin, C.-T. Huang, Y.-T. Chen, and C.-Y. Chiou, "Comparison of simulated power system dynamics applying various load models with actual recorded data," *IEEE Trans. Power Syst.*, vol. 9, no. 1, pp. 248–254, Feb. 1994.

[22] J. V. Milanovic, K. Yamashita, S. M. Villanueva, S. Z. Djokic, and L. M. Korunovi, "International industry practice on power system load modeling," *IEEE Trans. Power Syst.*, vol. 28, no. 3, pp. 3038–3046, Aug. 2013.

[23] "Load representation for dynamic performance analysis (of power systems)," *IEEE Trans. Power Syst.*, vol. 8, no. 2, pp. 472–482, May 1993.

[24] D. Kosterev *et al.*, "Load modeling in power system studies: WECC progress update," in *Proc. IEEE Power Energy Soc. Gen. Meeting*, Jul. 2008, pp. 1–8.

[25] Western Electricity Coordinating Council, "Composite Load Model for Dynamic Simulations," 2012. [Online]. Available: https://www.wecc.biz/_layouts/15/WopiFrame.aspx?sourcedoc=/Reliability/WECCemOpen=1

[26] North American Electric Reliability Corporation, "Dynamic Load Modeling," 2016. [Online]. Available: http://www.nerc.com/comm/PC/LoadModelingTaskForceDL/Dynamic deling

[27] Q. Liu, Y. Chen, and D. Duan, "The load modeling and parameters identification for voltage stability analysis," in *Proc. Int. Conf. Power Syst. Technol.*, vol. 4, 2002, pp. 2030–2033.

[28] J. Zhao, M. Netto, and L. Mili, "A robust iterated extended Kalman filter for power system dynamic state estimation," *IEEE Trans. Power Syst.*, vol. 32, no. 4, pp. 3205–3216, Jul. 2017.

[29] J. A. de Kock, F. S. van der Merwe, and H. J. Vermeulen, "Induction motor parameter estimation through an output error technique," *IEEE Trans. Energy Convers.*, vol. 9, no. 1, pp. 69–76, Mar. 1994.

[30] V. Knyazkin, C. A. Canizares, and L. H. Soder, "On the parameter estimation and modeling of aggregate power system loads," *IEEE Trans. Power Syst.*, vol. 19, no. 2, pp. 1023–1031, May 2004.

[31] T. Hiyama, M. Tokieda, W. Hubbi, and H. Andou, "Artificial neural network based dynamic load modeling," *IEEE Trans. Power Syst.*, vol. 12, no. 4, pp. 1576–1583, Nov. 1997.

[32] P. Ju, E. Handschin, and D. Karlsson, "Nonlinear dynamic load modelling: Model and parameter estimation," *IEEE Trans. Power Syst.*, vol. 11, no. 4, pp. 1689–1697, Nov. 1996.

[33] G. Giorgi and C. Narduzzi, "Performance analysis of Kalman-filter-based clock synchronization in IEEE 1588 networks," *IEEE Trans. Instrum. Meas.*, vol. 60, no. 8, pp. 2902–2909, Aug. 2011.

[34] C. Cortes and V. Vapnik, "Support vector networks," *Mach. Learn.*, vol. 20, no. 3, pp. 273–297, Sep. 1995.

[35] G. P. McCormick, *Nonlinear Programming: Theory, Algorithms, and Applications*. New York, NY, USA: Wiley, 1983.

[36] S. Bolognani, "Approximate linear solution of power flow equations in power distribution networks," 2015. [Online]. Available: https://github.com/saveriob/approx-pf

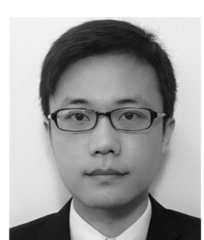

Chong Wang (M'16) received the B.E. and M.S. degrees in electrical engineering from Hohai University, Nanjing, China, in 2009 and 2012, respectively, and the Ph.D. degree in electrical engineering from The University of Hong Kong, Hong Kong, in 2016.

He was a Postdoctoral Researcher with The University of Hong Kong in 2016. From 2017 to 2018, he was a Postdoctoral Researcher with Iowa State University, Ames, IA, USA. He is currently an Associate Professor with the College of Energy and Electrical Engineering, Hohai University. His research interests include optimization and its applications in power systems, smart grids, integration of renewable energy sources, and cyber-physical systems.

Zhaoyu Wang (S'13–M'15) received the B.S. and M.S. degrees in electrical engineering from Shanghai Jiaotong University, Shanghai, China, in 2009 and 2012, respectively, and the M.S. and Ph.D. degrees in electrical and computer engineering from the Georgia Institute of Technology, Atlanta, GA, USA, in 2012 and 2015, respectively.

He is currently the Harpole-Pentair Assistant Professor with Iowa State University, Ames, IA, USA. He was a Research Aid with Argonne National Laboratory, Lemont, IL, USA, in 2013 and an Electrical Engineer Intern with Corning Inc., Corning, NY, USA, in 2014. His research interests include power distribution systems, microgrids, renewable integration, power system resilience, and power system modeling. He is the Principal Investigator for a multitude of projects focused on these topics and funded by the National Science Foundation, the Department of Energy, National Laboratories, PSERC, Iowa Energy Center, and Industry.

Dr. Wang was the recipient of the IEEE PES General Meeting Best Paper Award in 2017 and the IEEE Industrial Application Society Prize Paper Award in 2016. He is the Secretary of the IEEE Power and Energy Society Award Subcommittee. He is an Editor for the IEEE TRANSACTIONS ON SMART GRID and IEEE PES LETTERS.

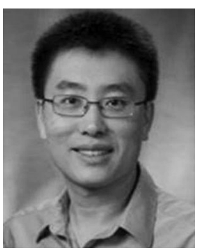

Jianhui Wang (M'07–SM'12) received the Ph.D. degree in electrical engineering from the Illinois Institute of Technology, Chicago, IL, USA, in 2007.

He is currently an Associate Professor with the Department of Electrical Engineering, Southern Methodist University, Dallas, TX, USA. Prior to joining SMU, he had a 11-year stint at Argonne National Laboratory, Lemont, IL, USA, with the last appointment as the Section Lead—Advanced Grid Modeling.

Dr. Wang is the Secretary of the IEEE Power & Energy Society (PES) Power System Operations, Planning & Economics Committee. He has held visiting positions in Europe, Australia, and Hong Kong, including a VELUX Visiting Professorship at the Technical University of Denmark, Copenhagen, Denmark. He is the Editor-in-Chief for the IEEE TRANSACTIONS ON SMART GRID and an IEEE PES Distinguished Lecturer. He was the recipient of the IEEE PES Power System Operation Committee Prize Paper Award in 2015.

Dongbo Zhao (S'10–M'14–SM'16) received the B.S. degree from Tsinghua University, Beijing, China, the M.S. degree from Texas A&M University, College Station, TX, USA, and the Ph.D. degree from the Georgia Institute of Technology, Atlanta, GA, USA, all in electrical engineering.

From 2014 to 2016, he was an R&D Engineer with Eaton Corporation and with ABB from 2010 to 2011. He is currently an Energy System Scientist with Argonne National Laboratory, Lemont, IL, USA. His research interests include power system control, protection, reliability analysis, transmission and distribution automation, and electric market optimization.

Dr. Zhao is a member of the IEEE PES Society, the Smart Grid Community, and the IEEE Young Professionals. He is an Associate Editor for *IET Renewable Power Generation*, an Editor for *International Transactions on Electrical Energy Systems*, and an Associate Editor for IEEE ACCESS.